Macromolecules

Article

pubs.acs.org/Macromolecules

Micellization of Binary Diblock Co-polymer Mixtures in an Ionic Liquid

- 3 Dan Zhao, To Yuanchi Ma, En Wang, and Timothy P. Lodge*, Lod
- ⁴ Department of Chemistry and [‡]Department of Chemical Engineering and Materials Science, University of Minnesota, Minneapolis,
- 5 Minnesota 55455, United States
- 6 Supporting Information

7

8

9

10

11

12

13

14

15

16

17

18

19

20

21 22

23

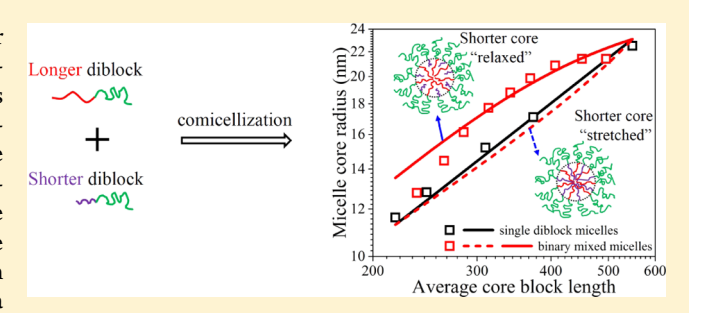
2.4

25 26

27

28

ABSTRACT: The structure of mixed diblock co-polymer micelles in the aprotic ionic liquid 1-ethyl-3-methylimidazo-lium bis(trifluoromethylsulfonyl)imide, [EMIM][TFSI], was investigated by dynamic light scattering (DLS), small-angle X-ray scattering (SAXS), and small-angle neutron scattering. The diblock co-polymers are poly(methyl methacrylate)-block-poly(n-butyl methacrylate) (PMMA-b-PnBMA), where PMMA is solvent selective and forms the corona of the micelles, whereas PnBMA segregates into the micelle core. In these experiments, a pair of diblocks with the same corona block length but distinct core block lengths ($N_{\rm core}$) was first



mixed homogeneously and then allowed to self-assemble into well-defined mixed micelles. DLS and SAXS measurements show that the hydrodynamic radius (R_h) and core radius (R_c) increase monotonically with the fraction of the longer diblock in the mixture. Interestingly, the dimensions of the binary mixed micelles are significantly larger than those formed by a single diblock with the same number average core block length $(\langle N_{core} \rangle)$. Similarly, the aggregation number is also much larger for the mixed micelles. These results can be understood by recognizing that in the binary mixed micelles, the shorter core blocks are not necessarily stretched to the center of the micelle core, which will be predominantly occupied by the longer core blocks. This relief of the shorter core block stretching effectively increases the aggregation number. Free-energy calculations confirm this hypothesis and are able to predict the R_c values of the binary mixed micelles quantitatively by eliminating the elastic free energy of the shorter core blocks. These results provide new physical insight into the micellization of binary co-polymer mixtures and demonstrate that block polymer blending is a facile strategy for precise tuning of the micellar structure (e.g., core radius and corona density).

INTRODUCTION

30 Block co-polymers (BCPs), which can self-assemble into various nanoscale micellar structures in a selective solvent, 1-3 32 offer advantages in diverse emerging technologies, including 33 drug and gene delivery, an anolithography, nanoreac-34 tors, oil recovery, and synthesis of mesoporous 35 materials. 15 For many of these applications, it is desirable to 36 control the micelle structure, such as the core dimension, the 37 interfacial area per chain, and the corona density. For instance, the micelle core/corona interfacial structure and the corona 39 density profile are critical factors affecting the transport of 40 small molecules into or out of the micelles, which in turn play 41 important roles in drug delivery and nanoreactor applications. 42 Additionally, the size of micelles determines their blood 43 circulation time as drug carriers. Moreover, it has been recently 44 shown that higher solvent (i.e., water) content in the micelle 45 corona (related to corona density) provides better micelle 46 mobility, leading to improved interaction with cell receptors 47 and, therefore, enhanced biological activity. 16

One common way to tune the micellar structure is to vary the BCP molecular characteristics (such as core and corona block length)^{2,17–20} and solvent selectivity. However, precise

structural control requires the synthesis of BCPs with exact 51 chain lengths and compositions. A more facile and efficient 52 way to tune the micelle structure is to blend BCPs with 53 different molecular characteristics or functionality. In fact, this 54 is a common strategy encountered in biological (e.g., lipids) 55 and industrial (e.g., surfactant) systems. Several additional 56 factors make the blending methodology attractive. First, other 57 thermodynamic properties, such as the critical micelle 58 concentration, critical micelle temperature (CMT), and the 59 gelation and rheological behavior of concentrated micelle 60 dispersions, can be manipulated by self-assembly of binary 61 BCP mixtures. 21-25 Second, micellization of binary BCP 62 mixtures can lead to distinct morphologies or structures that 63 cannot be achieved with single BCPs. 26-31 For instance, it has 64 been postulated that a binary mixture of two diblock co- 65 polymers with a common core block but incompatible corona 66 blocks might self-assemble into "patchy" micelles. 31 It has also 67 been shown that mixed micelles from BCPs provide superior 68

Received: March 26, 2019 Revised: May 22, 2019



69 physical stability and redispersion properties, which can 70 enhance their application in drug delivery. Third, blends 71 of amphiphilic molecules are commonly formulated and used 72 in commercial practice, since it is difficult to recycle and 73 separate mixtures of surfactants or BCPs.

Micellization of binary BCP mixtures has been extensively rs investigated by theory, 33-35 simulation, 36-38 and experiment. 76 Measurements have been conducted in aqueous solutions 77 (particularly Pluronics in water), 21-23,39-41 organic sol-78 vents, 42-46 and very recently in a protic ionic liquid (IL).47 79 Among these studies, the two BCPs could differ in core block 80 length, core block chemistry, corona block length, or corona 81 block chemistry. Here, we highlight the previous work on self-82 assembly of binary BCPs of identical chemical nature and 83 corona block length but distinct core block lengths. In general, 84 the two co-polymers could assemble into monomodal mixed 85 micelles (with uniform composition) or demixed ones with a 86 bimodal distribution (the two populations could be pure and 87 mixed micelles or both mixed ones with distinct composi-88 tions). This depends primarily on the difference between the 89 core block lengths, the stoichiometry of the binary mixture, 90 and the process of micellization. Specifically, the theory 91 predicts that when the core block lengths are similar, only 92 mixed micelles are stable, but when the difference is large, 93 mixed micelles co-exist with pure micelles. 33,35 This prediction 94 was experimentally confirmed by Gaisford et al. using iodine 95 incorporation UV spectroscopy. The proportion of the two 96 BCPs in the mixture also plays a role. It was reported that co-97 micellization becomes more favorable when the two polymer 98 species have similar concentrations. 35,37,42 In contrast, when 99 the relative fraction of the shorter chains in the mixture is high, 100 the excess short chains form pure micelles, leading to the co-101 existence of two types of micelles. 42,48 On the other hand, in 102 practice, the formation of either mixed or demixed micelles is also dictated by the sample processing history, presumably as a 104 consequence of nonergodicity. 26,42,43 For instance, Jain et al. 105 found that although the premixing protocol (i.e., mix the two 106 co-polymers homogeneously before micellization) yields mixed 107 micelles, postmixing of the individual BCP dispersions 108 produces morphologies representing a superposition of the 109 two pure BCP solutions (i.e., unmixed micelles). 26 Honda et 110 al. studied the micellization of binary BCP mixtures with 111 different CMTs after single-step or double-step temperature 112 jumps (T-jumps) from the unimer region. It was reported that 113 in a single-step *T*-jump, where both co-polymers form micelles, 114 co-micellization takes place. In a double-step T-jump, first from 115 a unimer region to an intermediate temperature at which only 116 one co-polymer forms micelles and subsequently to a region 117 where both co-polymers form micelles, two populations of 118 micelles were observed. 42 Due to these thermodynamic and 119 kinetic factors, both mixed and unmixed micelles have been 120 reported in the literature. For example, a bimodal distribution 121 of micelles was confirmed by microdifferential scanning 122 calorimetry, transmission electron microscopy (TEM), and 123 dissipative particle dynamics simulations. 22,37,43,46 In contrast, 124 in many other studies, the two BCPs were found to fully 125 hybridize into mixed micelles. 25,26,36,38,40,41,49 In general, the 126 structural parameters of the mixed micelles (e.g., hydro-127 dynamic radius, core radius, and aggregation number) are 128 intermediate between those formed with individual BCP 129 chains. However, due to the limited resolution of the 130 experiments and the small difference between the two BCPs 131 used, the exact relation between the micelle dimensions and

the average core block length ($\langle N_{\rm core} \rangle$) has not been 132 established. Additionally, although in some cases, one clearly 133 sees systematic deviations of the structural or dynamic 134 characteristics of the mixed micelles from those expected for 135 pure micelles with an equal $\langle N_{\rm core} \rangle$, 26,36,41,48,50 a good 136 understanding of these observations is missing. Moreover, 137 how the micelle core radius depends on the proportion of the 138 two BCPs has not been directly probed.

To address these interesting questions, we report the 140 micellization of binary mixtures of poly(methyl methacry- 141 late)-block-poly(n-butyl methacrylate) (PMMA-b-PnBMA) di- 142 block co-polymers in 1-ethyl-3-methylimidazolium bis- 143 (trifluoromethylsulfonyl)imide, [EMIM][TFSI]. As shown in 144 our previous studies, 51,52 PMMA is the solvent-selective block 145 and forms the micelle corona, whereas PnBMA, displaying a 146 lower critical solution temperature (LCST) in [EMIM][TFSI], 147 forms the micelle core. The two diblocks have the same corona 148 block length (N_{corona}) but different core block lengths (N_{core}). 149 Each pair of diblocks studied here co-assemble into mixed 150 micelles at all proportions. The structure of the formed mixed 151 micelles is characterized by a combination of dynamic light 152 scattering (DLS), small-angle X-ray scattering (SAXS), and 153 small-angle neutron scattering (SANS). Due to the relative 154 monodispersity and good scattering contrast, the micelle core 155 radius can be precisely determined by SAXS or SANS. The 156 measurements were performed at 55 °C, which is ~130-180 157 °C above the LCST of PnBMA in [EMIM][TFSI].53 158 Additionally, the experimental temperature is much higher 159 than the glass transition temperature (T_g) of the solvophobic 160 PnBMA block ($T_{\rm g} \approx 20$ °C),⁵⁴ thus the kinetically trapped ¹⁶¹ states associated with a glassy, frozen micelle core can be ¹⁶² circumvented.⁵⁵ The results are interpreted in detail using an 163 extension of the classical micelle free-energy balance.^{3,56,5}

EXPERIMENTAL SECTION

Synthesis and Characterization. Sequential radical addition— 166 fragmentation chain-transfer polymerization was used to synthesize a 167 series of diblock co-polymers of PMMA-b-PnBMA, with the details 168 provided in a previous report. Earliefly, the PMMA block was first 169 prepared and following that the PnBMA block was grown from the 170 PMMA macrochain transfer agent. The number-averaged molecular 171 weight (M_n) of the PMMA block and the dispersity (D) of the 172 diblocks were obtained from size exclusion chromatography (SEC) 173 with a multiangle laser light scattering detector (Wyatt DAWN). The 174 M_n of the PnBMA block was determined by H nuclear magnetic 175 resonance spectroscopy (H NMR, Varian Inova 500). The molecular 176 characteristics of the diblocks are presented in Table 1. The IL 177 till

Table 1. Molecular Parameters of Diblock Co-polymers

PMMA-b-PnBMA	$M_{n,PMMA}^{c}$ (kg/mol)	$M_{n,P_{n}BMA}^{c}$ (kg/mol)	$N_{\mathrm{PMMA}}^{}d}$	$N_{ m PnBMA}^{d}$	D^e
$(25-24)^a$	25	24	250	169	1.05
$(25-31)^{b}$	25	31	250	218	1.05
$(25-35)^{b}$	25	35	250	246	1.05
$(25-44)^{b}$	25	44	250	310	1.07
$(25-50)^a$	25	50	250	352	1.08
$(25-53)^{b}$	25	53	250	373	1.07
$(25-78)^{b}$	25	78	250	549	1.11

"The SEC traces of these two diblocks are shown in Figure S1. ^bAs reported previously. ⁵² $^cM_{n,PMMA}$ and $M_{n,PnBMA}$ are number-averaged molecular weights of the individual blocks. $^dN_{PMMA}$ and N_{PnBMA} are the degrees of polymerization of the two blocks. cD ispersity of the diblock co-polymer.

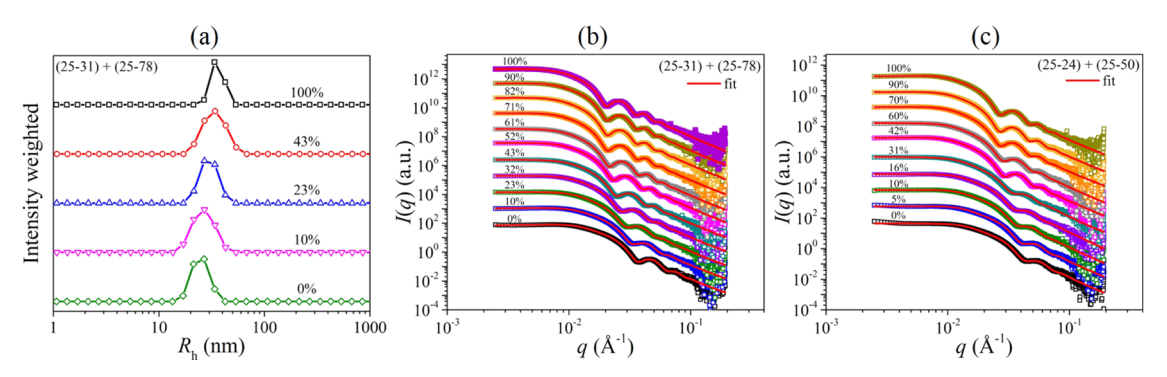


Figure 1. (a) Representative hydrodynamic radius distributions at $\theta = 90^{\circ}$ for 0.5 wt % mixed micelle solutions of (25-31) + (25-78) in [EMIM][TFSI]. The weight fractions of the longer diblock (25-78) in the co-polymer mixture are indicated inside the graph. SAXS intensity I(q) vs scattering vector q for 1 wt % binary mixed micelles of (b) ((25-31) + (25-78)) and (c) ((25-24) + (25-50)) in [EMIM][TFSI]. The weight fractions of the longer diblock in the co-polymer mixture are indicated inside the graph. The symbols represent the experimental data, and the red lines are best fits to the Pedersen model with the Percus–Yevick structure factor. The scattering traces were vertically shifted by factors of 10 for clarity.

178 [EMIM][TFSI] was synthesized by the ion-exchange reaction of 179 [EMIM]Br and Li[TFSI] at 70 °C for 24 h. To enhance the contrast 180 in the neutron scattering experiment, partially deuterated [EMIM]-181 [TFSI] was also prepared via the isotopic exchange of the three 182 hydrogens on the imidazole ring with deuterated water at 100 °C for 183 3 days. All other chemicals were obtained from Sigma-Aldrich.

Sample Preparation. All mixed micellar solutions in the IL were prepared with a polymer concentration of 0.5 or 1 wt % using a cosolvent. Mixtures of the two diblock co-polymers with a known proportion together with an appropriate amount of IL were first dissolved in dichloromethane (DCM). The co-solvent was slowly 188 189 removed via nitrogen purge until no change in the solution weight was observed, during which the block co-polymer micelles were formed. Following that the resulting micellar solution was kept at 50 °C for 12 h under vacuum (<100 mTorr) to completely remove any 193 residual co-solvent. To examine the effect of the sample preparation protocol, some samples with a similar co-polymer ratio and 194 concentration were made by the following process. First, separate 195 196 micellar solutions were prepared for the two diblocks following the co-solvent method described above. Subsequently, the two micellar solutions were mixed in a predetermined ratio in the co-solvent. The 199 mixed micelles were finally formed via removal of the co-solvent. Similar results were obtained from both protocols, as discussed below. 200

Dynamic Light Scattering (DLS). A multiangle light scattering 201 202 instrument (Brookhaven BI-200SM, with a laser wavelength of 637 203 nm) was used to conduct the DLS measurements. In a typical experiment, the micelle solution (concentration 0.5 or 1 wt %) was filtered with a 0.45 μ m PTFE filter into a glass tube, which was then connected to a vacuum line to remove any air bubbles, and finally sealed with parafilm. All of the DLS experiments were performed at 55 °C, and all of the micelle solutions were thermally equilibrated at this temperature for at least 10 min before data acquisition. Intensity 210 autocorrelation functions, $g^{(2)}(t)$, were collected at multiple angles from 50 to 130°, with 20° intervals, for 10 min each. Each correlation 212 function was first analyzed by inverse Laplace transform using the 213 regularized positive exponential sum (REPES) method to obtain the 214 hydrodynamic radius distribution.⁵⁸ Note that in all of the micelle 215 solutions studied, there is only a single population of micelles with a 216 relatively narrow distribution. Thus, the $g^{(2)}(t)$ could also be analyzed 217 by the second-order cumulant method. From this analysis, the average 218 decay rate $(\overline{\Gamma})$ was extracted, from which the diffusion coefficient 219 (D_m) was obtained from a linear fit of $\overline{\Gamma}$ vs q^2 . Here, q is the scattering 220 vector, given by $q = (4\pi n/\lambda)\sin(\theta/2)$, n is the refractive index of the 221 IL at 55 °C, λ is the vacuum wavelength of the laser, and θ is the 222 scattering angle. Additionally, the size dispersity $(\mu_2/\overline{\Gamma}^2)$ of the 223 micelles was assessed from the normalized second cumulant. Finally, 224 the Stokes-Einstein relation was used to calculate the average 225 hydrodynamic radius (R_h) of the micelles, given as $R_h = k_B T/$

 $(6\pi\eta D_{\rm m})$, where $k_{\rm B}$ is the Boltzmann constant, T is the absolute 226 temperature, and η is the viscosity of the IL at 55 °C.

Small-Angle X-ray Scattering (SAXS). The SAXS data were 228 collected on the 5-ID-D beamline (Dupont-Northwestern-Dow 229 Collaborative Access Team) at the Advanced Photon Source, 230 Argonne National Laboratory. The wavelength was 0.73 Å and the 231 sample-to-detector distance for the small-angle scattering config- 232 uration was 8.50 m, which provided a q range of $\sim 0.0025 - 0.19 \text{ Å}^{-1}$. 233 For the measurements, the micelle solutions were transferred into 234 quartz capillary tubes (~1.5 mm in diameter) and then sealed with 235 epoxy. All of the experiments were conducted at 55 °C. A Rayonix 236 CCD area detector was used to collect the two-dimensional (2D) 237 scattering data, with a typical acquisition time of 0.5 or 1 s. The 2D 238 isotropic scattering data were then converted into one-dimensional 239 (1D) traces (I(q) vs q) via an azimuthal average. The scattering of the 240 IL in the capillary tube was also collected as the background. The 241 Pedersen model for block co-polymer micelles with the Percus- 242 Yevick hard sphere structure factor was used to analyze the scattering 243

Small-Angle Neutron Scattering (SANS). The SANS measure- 245 ments were conducted on the NG7 30 m SANS beamline at the 246 Center for Neutron Research of the National Institute of Standards 247 and Technology (NIST). The wavelength of the neutron beam was 248 6.0 Å, with a spread $(\Delta \lambda/\lambda)$ of 0.115. Three configurations (with 249 sample-to-detector distances of 1, 4, and 13 m) were combined to 250 provide a q range of $\sim 0.0039-0.56$ Å $^{-1}$. In typical runs, the micelle 251 solutions were transferred into 1 mm banjo cells and then placed on 252 the beamline for data collection. All measurements were performed at 253 S5 °C. The 2D scattering data at each configuration were separately 254 reduced and converted to 1D profiles using the Igor Pro package 255 developed by NIST. The obtained 1D data at all configurations 256 were then merged and analyzed by the same scattering model as in 257 SANS

■ RESULTS AND DISCUSSION

Figure 1a shows the intensity-weighted hydrodynamic radius 260 ft distributions at $\theta = 90^{\circ}$ for 0.5 wt % mixed micelles of (25-26131) + (25-78) with varying proportions in [EMIM][TFSI] at 262 55 °C, obtained from the REPES analysis. There is a single, 263 narrowly distributed population in micelles formed with either 264 a single diblock or a binary mixture of two diblocks, indicating 265 the formation of mixed micelles. 21,40,42 As the fraction of the 266 longer diblock increases, the peak hydrodynamic radius of the 267 mixed micelles grows monotonically. For instance, it increases 268 from 23.8 to 32.6 nm when the weight fraction of (25-78) is 269 raised from 0 to 43%. Additionally, the intensity correlation 270 function $g_1^{-2}(t)$ (Figure S2) of each micelle solution can be well 271

259

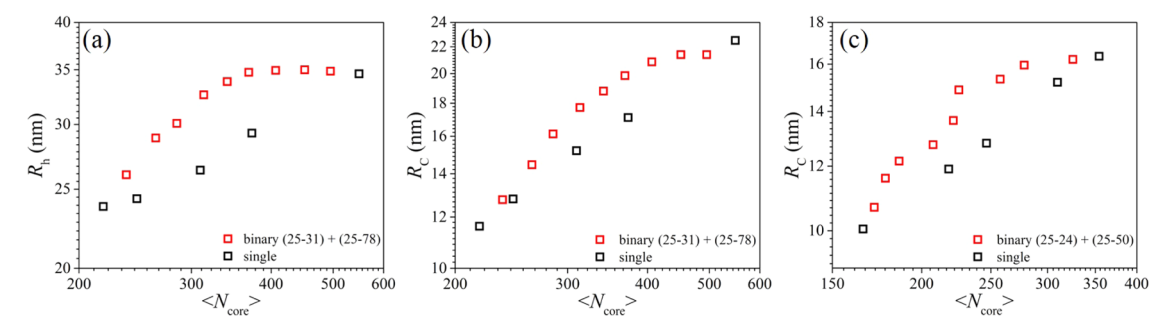


Figure 2. (a) Hydrodynamic radius R_h vs the average core block length $\langle N_{\text{core}} \rangle$ for 0.5 wt % micelle solutions in [EMIM][TFSI]. (b, c) Micelle core radius R_c vs $\langle N_{\text{core}} \rangle$ for 1 wt % micelle solutions in [EMIM][TFSI]. The black squares correspond to micelles formed with a single diblock copolymer, whereas the red ones represent mixed micelles of (b) (25-31) + (25-78) and (c) (25-24) + (25-50).

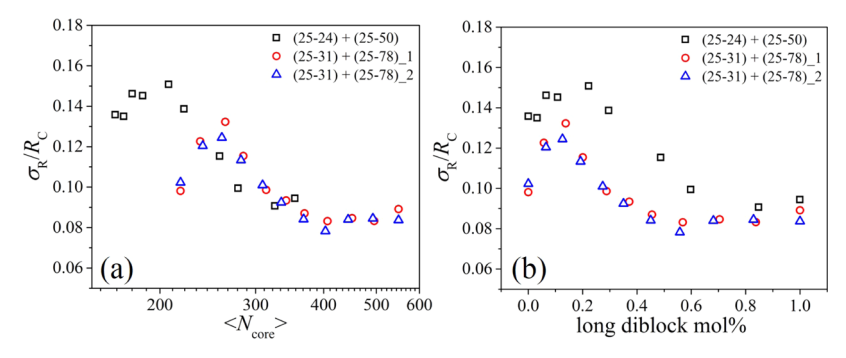


Figure 3. (a) Coefficient of variation σ_R/R_c vs $\langle N_{\rm core} \rangle$ for 1 wt % binary diblock co-polymer micelles in [EMIM][TFSI]. The "(25–31) + (25–78) _1" and "(25–31) + (25–78) _2" were prepared following two different protocols, as described in the Experimental Section. (b) The same data in (a) plotted vs the mole fraction of the longer diblock.

272 described by the second-order cumulant expansion, with the 273 obtained decay rate $\overline{\Gamma}$ plotted as a function of q^2 in the inset of 274 Figure S2. Clearly, as shown there, $g_1^2(t)$ decays at later times 275 with the increase in the weight fraction of (25-78) in the co-276 polymer mixture, indicating a larger micelle size, consistent 277 with Figure 1a. The linear fits of $\overline{\Gamma}$ vs q^2 yield the diffusion 278 coefficient of the micelles and from there R_h can be obtained. 279 The mean R_h is shown in Figure 2a as a function of the average 280 core block length $\langle N_{\rm core} \rangle$, defined by

$$\langle N_{\text{core}} \rangle = \overline{x_{\text{L}}} N_{\text{core,L}} + (1 - \overline{x_{\text{L}}}) N_{\text{core,S}}$$
 (1)

$$\overline{x_{\rm L}} = \frac{\omega_{\rm L}/M_{\rm n,L}}{\omega_{\rm L}/M_{\rm n,L} + (1 - \omega_{\rm L})/M_{\rm n,S}} \tag{2}$$

where $\overline{x_L}$ is the mole fraction of the longer diblock in the co-284 polymer mixture, $N_{\text{core,L}}$ and $N_{\text{core,S}}$ are the core block lengths 285 of the longer and shorter diblock, respectively, $\omega_{\rm L}$ is the weight 286 fraction of the longer diblock in the mixture, $M_{\rm n,L}$ and $M_{\rm n,S}$ are 287 the molecular weights of the longer and shorter diblocks, 288 respectively, which are equal to 103 and 56 kg/mol for the 289 diblock pair of (25-78) and (25-31). As shown in Figure 2a, 290 the average R_h of the binary mixed micelles increases monotonically with $\langle N_{\rm core} \rangle$. Moreover, the dispersity of the 292 hydrodynamic radius $(\mu_2/\overline{\Gamma}^2)$ is smaller than 0.1 for all of the 293 micelles (Figure S3), confirming that the two diblocks formed 294 mixed micelles with a single population. 42 Figure 2a also shows 295 $R_{\rm h}$ for single component micelles, with different core block 296 lengths. As expected, with the increase of the core block length, 297 the micelle size becomes larger. Interestingly, for a given ²⁹⁸ $\langle N_{\rm core} \rangle$, the $R_{\rm h}$ of the mixed micelles is significantly larger than 299 for the pure micelles. For example, at $\langle N_{\rm core} \rangle \approx 370$, $R_{\rm h} = 29.3$ 300 and 34.7 nm, respectively, for the pure and mixed diblock copolymer micelles. Similar results were obtained for another pair $_{301}$ of diblocks, (25-24) + (25-50) (Figure S4). The underlying $_{302}$ mechanism for these intriguing findings will be discussed later. $_{303}$

We next compare the core dimensions of the mixed micelles 304 to pure micelles. Figure 1b,c shows scattering profiles of mixed 305 micelles of (25-31) + (25-78) and (25-24) + (25-50), 306 respectively, in [EMIM][TFSI] at 1 wt %. For each trace, the 307 scattering intensity oscillates in the high q regime and levels off 308 at lower values of q, characteristic of spherical micelles without 309 any larger-scale aggregates in the solution. As the scattering 310 contrast results primarily from the core, 63 the micelle core 311 radius R_c can be inferred from the position of the first q 312 minimum $(q_{1,min})$. As shown in Figure 1b,c, in both pairs of 313 diblocks, as the weight fraction of the longer diblock increases, 314 $q_{1,\min}$ systematically shifts to lower q values, indicating larger 315 core sizes. The scattering data can be well described by the 316 Pedersen model combined with the Percus-Yevick structure 317 factor, from which R_c can also be determined; the results are 318 plotted against $\langle N_{\rm core} \rangle$ in Figure 2b,c. Note that the values of 319 $R_{\rm c}$ extracted from the fittings and that from the characteristic 320 equation for the minima in q (i.e., $q_{1,min}R_c = 4.49$) agree very 321 well (Figure S5). Additionally, to check the reproducibility of 322 the measurements and to evaluate the effect of sample 323 preparation, we prepared another set of mixed micelle 324 solutions of (25-31) + (25-78) by first preforming two 325 pure diblock co-polymer micelles, then blending the two 326 micelles in DCM and finally forming the mixed micelles via 327 removal of DCM. This protocol also yields well-defined 328 spherical micelles (Figure S6). Moreover, the core dimensions 329 of the mixed micelles prepared by the two different methods 330 are nearly the same (Figure S5b), supporting the robustness of 331 the sample preparation and measurements.

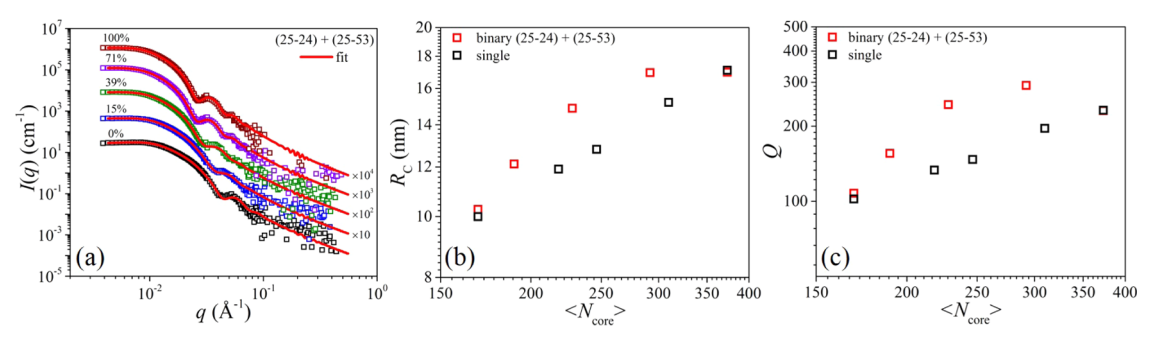


Figure 4. (a) SANS intensity I(q) vs scattering vector q for 1 wt % binary diblock co-polymer ((25–24) + (25–53)) micelles in partially deuterated [EMIM][TFSI]. The weight fractions of (25–53) in the co-polymer mixture are indicated. The symbols represent the experimental data, and the red lines are best fits to the Pedersen model with the Percus–Yevick structure factor. The scattering traces were vertically shifted for clarity. (b) R_c vs $\langle N_{core} \rangle$ and (c) the micelle aggregation number Q vs $\langle N_{core} \rangle$ for 1 wt % micelle solutions in partially deuterated [EMIM][TFSI]. The black squares represent experimental data of single diblock co-polymer micelles adapted from a previous report, whereas the red ones correspond to the binary mixed micelles. For the single diblock micelles, Q was estimated from the SAXS R_c values assuming that there is \sim 10 vol % solvent in the micelle core.

Figure 2b,c presents R_c vs $\langle N_{core} \rangle$ for binary mixed micelles 334 of (25-31) + (25-78) and (25-24) + (25-50), respectively. 335 In both cases, R_c increases monotonically with $\langle N_{core} \rangle$. This 336 agrees well with the change in $q_{1,min}$ in Figure 1b,c as well as 337 the trend of $R_{\rm h}$ with $\langle N_{\rm core} \rangle$ in Figures 2a and S4. Figure 2b,c $_{338}$ also includes $R_{\rm c}$ of pure micelles adapted from an earlier 339 work. S2 As reported previously, the R_c of single diblock 340 micelles scales as $\langle N_{\rm core} \rangle^{0.71}$; in contrast, R_c of the binary mixed 341 micelles vs $\langle N_{\rm core} \rangle$ does not follow a power law. Instead, $R_{\rm c}$ $_{342}$ increases more rapidly at smaller values of $\langle N_{\rm core} \rangle$ and nearly 343 plateaus when $\langle N_{\rm core} \rangle$ approaches that of the longer diblock. 344 Consistent with the behavior of $R_{\rm h}$, $R_{\rm c}$ of the mixed micelles is significantly larger than for pure micelles at the same $\langle N_{\rm core} \rangle$. A 346 similar result was found by Jain et al. for micelles with a 347 spherical morphology. 26 Figure 3a shows the coefficient of variation in R_c (CV = σ_R/R_c) as a function of $\langle N_{\text{core}} \rangle$. In mixed 349 micelles formed with both pairs of diblocks, there is an 350 apparent maximum in σ_R/R_c , which occurs roughly near 15 351 mol % of the longer diblock in both cases, as shown in Figure 352 3b. This result will be discussed subsequently.

We examine the aggregation number of the binary mixed 354 micelles based on the SANS measurements. Figure 4a presents 355 the neutron scattering intensity I(q) vs scattering vector q for 356 mixed micelles of (25-24) + (25-53) in partially deuterated [EMIM][TFSI]. Consistent with the SAXS data, $q_{1,min}$ clearly 358 decreases with increasing fraction of the longer diblock, again R_c . The SANS traces were also well fit 360 by the Pedersen model with a hard sphere structure factor, 361 from which R_c and the micelle aggregation number Q can be 362 simultaneously determined. Consistently, R_c increases with $_{363}$ $\langle N_{\rm core} \rangle$, and it is significantly larger for the binary mixed 364 micelles than pure ones at the same $\langle N_{\rm core} \rangle$ (Figure 4b). 365 Interestingly, in Figure 4c, we see that Q first increases and 366 then decreases with $\langle N_{\rm core} \rangle$. This indicates that at some 367 intermediate fraction of the longer diblock, one mixed micelle 368 contains more co-polymer chains than that formed with only 369 the longer diblock co-polymer. Similarly, Newby et al. 370 observed that the hydrodynamic radius of a 50/50 binary co-371 polymer mixture is larger than either pure micelles, which they 372 attributed to a higher aggregation number for the mixed 373 micelles. 50 This is consistent with the observation in Figure 4c. 374 Going further, similar to R_c , Q of the mixed micelles is much 375 larger than for single diblocks (estimated from the SAXS R 376 data assuming that there is \sim 10 vol % solvent in the micelle core, Figure S7). To summarize, by combining three different 377 scattering techniques, we consistently show that the micelle 378 dimensions can be precisely tuned by blending two diblock co- 379 polymers, with the values of the micelle size systematically 380 increasing with the fraction of the longer diblock. Importantly, 381 the micelle size (both $R_{\rm h}$ and $R_{\rm c}$) and the aggregation number 382 are significantly larger for the binary mixed micelles than for 383 those formed with a single diblock co-polymer. In the 384 following, free-energy calculations on both pure and mixed 385 micelle systems are performed to reveal the underlying 386 mechanism for these intriguing results.

We start from the single diblock co-polymer micellar system. 388 We adopt the theory developed by Zhulina et al., which 389 explicitly takes all contributions (core, corona, and interface) 390 to the free energy of the micelle into account. This allows the 391 model to be applicable to the crossover regime between the 392 crew-cut and starlike micelles, appropriate for the current 393 system. Moreover, the numerical coefficients for all of the free-energy terms were calculated from theory. According to this 395 model, the free energy per co-polymer chain (F_{chain}) within the 396 micelle is given by

$$\frac{F_{\text{chain}}}{k_{\text{B}}T} = \frac{4\pi R_{\text{c}}^{2} \gamma}{Q a_{\text{B}}^{2}} + \frac{3\pi^{2} R_{\text{c}}^{2}}{80 N_{\text{core}} b^{2}} + \frac{1}{2\sqrt{3}} C_{\text{E}} p_{\text{A}}^{-3/4}
- \frac{R_{\text{c}}^{3/2} \varphi^{1/2}}{N_{\text{core}}^{1/2} a_{\text{B}}^{3/2}} \ln \left[1 + \frac{2C_{\text{H}} p_{\text{A}}^{1/4} N_{\text{corona}} \varphi^{1/2} a_{\text{A}}^{2}}{\sqrt{3} R_{\text{c}}^{1/2} N_{\text{core}}^{1/2} a_{\text{B}}^{3/2}} \right]
+ F_{\text{chain,0}}$$
(3) 30

where $\gamma = (\gamma_{\rm BaB}^2)/(k_{\rm B}T)$ is the normalized interfacial tension at 399 the micelle core/corona interface, $\gamma_{\rm B}$ is the surface free energy 400 per unit area; $a_{\rm A}=0.52$ nm and $a_{\rm B}=0.6$ nm are the volumetric 401 sizes of one repeat unit of the corona and core block, 402 respectively; b=0.61 nm is the statistical segment length of the 403 core block; 65 $p_{\rm A}=1.44$ is the corona chain stiffness parameter; 404 $\varphi\approx0.9$ is the volume fraction of the core block in the micelle 405 core (Figure S7). Calculation of these parameters is shown in 406 Supporting Information. $F_{\rm chain,0}$ accounts for the free energy 408 difference state and also any other Q-independent free-energy 408 difference between the micelle and the reference states (e.g., 409 the enthalpy of mixing for the core block). As described by 410 Zhulina et al., 3 $C_{\rm F}$ and $C_{\rm H}$ depend on the solvent quality of the 411 corona block; eq 3 was derived for micelles in a θ solvent or 412

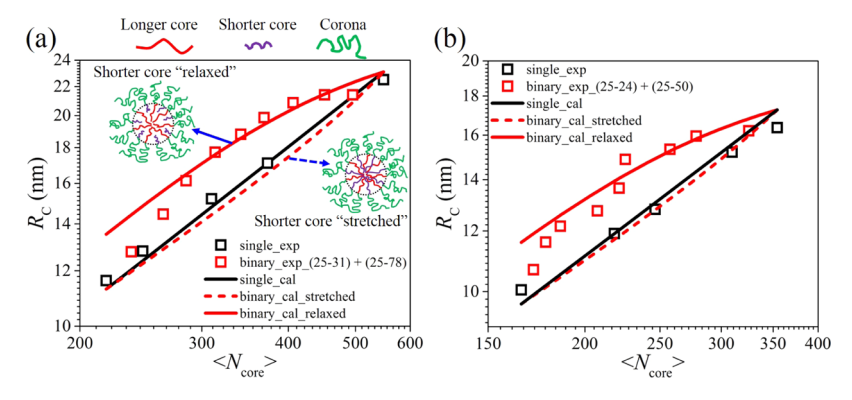


Figure 5. R_c extracted from the SAXS data vs $\langle N_{\rm core} \rangle$ for 1 wt % micelle solutions in [EMIM][TFSI], including binary mixed micelle of (a) (25–31) + (25–78) and (b) (25–24) + (25–50). In both (a) and (b), the black squares represent R_c of single diblock micelles and the red squares are the binary mixed ones. The solid black and dashed red lines are the free-energy calculations for single and binary diblock micelles, respectively, under the assumption that all core blocks are uniformly deformed to fill the micelle core. The solid red line is the free-energy calculation for the binary mixed micelles assuming no stretching of the shorter core block. The cartoons in (a) depict the "stretched" and "relaxed" conformations of the shorter core block, where the red, purple, and green lines correspond to the longer core block, shorter core block, and the corona block, respectively.

 $_{413}$ when the corona chain conformation is not significantly $_{414}$ modified by the excluded volume interactions. As the corona $_{415}$ block in the current work is relatively short, eq 3 is applicable $_{416}$ (see the justification in the Supporting Information). In fact, the exact expressions for $C_{\rm F}$ and $C_{\rm H}$ are not important for our $_{418}$ purpose as they will be estimated by fitting to the experiments. The first term on the right-hand side of eq 3 is the micellar $_{420}$ interfacial energy, the second term is the entropic stretching $_{421}$ penalty for the core block, and the third term represents the $_{422}$ free energy of the corona block (elastic free energy and $_{423}$ excluded volume interactions). Additionally, Q and $R_{\rm c}$ are $_{424}$ related by

$$\frac{4}{3}\pi R_{\rm c}^{3} \varphi = Q N_{\rm core} a_{\rm B}^{3} \tag{4}$$

426 By minimizing the free energy in eq 3 with respect to R_c

$$\frac{d\left(\frac{F_{\text{chain}}}{k_{\text{B}}T}\right)}{dR_{\text{c}}} = 0 \tag{5}$$

the equilibrium values of $R_{\rm c}$ can be obtained. To perform the calculation in eq 5, there are still three unknown parameters (γ , q_{30} $C_{\rm F}$, and $C_{\rm H}$), which we determine from the comparison with the experimental data of single diblock micelles. Figure S8 shows that the calculations from eq 5 agree very well with the experimental data (also shown by the solid black lines in Figure 5). From here, we obtain $\gamma = 0.096$, $C_{\rm F} = 1.40$, $C_{\rm H} = 0.06$, and summarize the model parameters in eq 3 in Table S1 in the Supporting Information. Note that these parameters are quite similar with those obtained in the literature 3,18 and will 438 be fixed in the following calculations.

 $_{439}$ We next consider the binary diblock co-polymer mixed $_{440}$ micelle system. In this case, additional terms need to be $_{441}$ included for the free energy of one block co-polymer chain, as $_{442}$ given by

$$\frac{F_{\text{chain}}}{k_{\text{B}}T} = \frac{4\pi R_{\text{c}}^{2} \gamma}{Q a_{\text{B}}^{2}} + x_{\text{S}} \frac{3\pi^{2} R_{\text{c}}^{2}}{80 N_{\text{core,S}} b^{2}} + x_{\text{L}} \frac{3\pi^{2} R_{\text{c}}^{2}}{80 N_{\text{core,L}} b^{2}}
+ \frac{1}{2\sqrt{3}} C_{\text{F}} p_{\text{A}}^{-3/4} \frac{R_{\text{c}}^{3/2} \varphi^{1/2}}{\langle N_{\text{core}} \rangle^{1/2} a_{\text{B}}^{3/2}}
\ln \left[1 + \frac{2C_{\text{H}} p_{\text{A}}^{1/4} N_{\text{corona}} \varphi^{1/2} a_{\text{A}}^{2}}{\sqrt{3} R_{\text{c}}^{1/2} \langle N_{\text{core}} \rangle^{1/2} a_{\text{B}}^{3/2}} \right] + \frac{\phi_{\text{S}}}{N_{\text{core,S}}} \ln(\phi_{\text{S}})
+ \frac{\phi_{\text{L}}}{N_{\text{core,L}}} \ln(\phi_{\text{L}}) + F_{\text{chain,0}} \tag{6}$$

where Q is the total aggregation number of one mixed micelle, 444 including both shorter and longer diblocks, x_S and x_L are the 445 mole fractions of the shorter and longer diblock co-polymer 446 chains in one mixed micelle; $x_{\rm S}$ + $x_{\rm L}$ = 1. Here, it is assumed 447 that the two diblocks are completely mixed, i.e., there is single 448 population of micelles and the composition of the two diblocks 449 in each micelle is the same, which can be known from the 450 blending formulation (i.e., $x_{\rm L} = \overline{x_{\rm L}}$). $\phi_{\rm S}$ and $\phi_{\rm L}$ are the volume 451 fractions of shorter and longer diblocks in one mixed micelle. 452 Thus, the two terms containing volume fractions in eq 6 453 account for the mixing entropy of the two diblocks in the 454 mixed micelle core. As we assume that the composition of the 455 two diblocks is constant among the micelles, these two terms 456 will not affect the minimization of the free energy. In eq 6, we 457 essentially separate the core free energy into two terms, one for 458 the longer core block and the other for the shorter core block. 459 For the calculation of the corona free energy, the average core 460 block length $\langle N_{\rm core} \rangle$ was used. Additionally, in the binary 461 mixed micelle we have

$$\frac{4}{3}\pi R_{c}^{3} \varphi = Q(x_{S} N_{\text{core},S} a_{B}^{3} + x_{L} N_{\text{core},L} a_{B}^{3})$$
(7) ₄₆₃

Similarly, by minimizing the free energy in eq 6 with respect to 464 R_{\odot} the core radius of the mixed micelles at equilibrium can be 465 predicted, as shown by the dashed red lines in Figure 5. These 466 calculations significantly underestimate the experimental values 467 in both binary mixed micelle systems and are even smaller than 468 the calculations of the single diblock micelles. This is because 469 in this calculation, it is assumed that both the shorter and 470 longer core blocks are uniformly stretched to fill the micelle 471

472 core, which favors a smaller micelle size to reduce the 473 stretching of the shorter core block, considering the fact that 474 the core block is significantly stretched in the micelle core in 475 the current system $(R_{\rm c} \sim N_{\rm core}^{-0.71})^{.52}$ However, for spherical 476 micelles, not all of the core blocks are necessarily stretched to 477 fill the central space of the micelle core. This is especially true 478 for the binary mixed micelle case, in which the longer core 479 blocks can relatively easily reach the center of the micelle, 480 making the shorter ones essentially relaxed. To explore this 481 physical picture, we removed the shorter core elastic free 482 energy in eq 6 (i.e., make the second term on the right-hand 483 side of eq 6 equal to zero) and performed the same free-energy 484 minimization calculation. The new predictions are represented 485 by the solid red lines in Figure 5. As expected, when there is no 486 elastic penalty for the shorter core blocks, larger values of R_c 487 are obtained. Interestingly, reasonable agreement is achieved 488 between the calculations and the experiments (except at 489 smaller $\langle N_{\rm core} \rangle$), justifying the physical picture proposed. This 490 idea can be further elaborated from the distribution of the core 491 block free ends. According to the calculation of Semenov, ⁶⁴ in 492 pure micelles, the density of core block end monomers 493 maximizes in the central part of the core and progressively 494 decreases in regions further away from the micelle core center. 495 In the mixed micelles, although the end monomer density 496 profile remains roughly the same for the longer core blocks as 497 that in pure micelles, the free ends of the shorter core blocks 498 should concentrate around some radial distances (presumably 499 close to the unperturbed end-to-end dimension) from the 500 micelle core/corona interface. This interpretation is corrobo-501 rated by the Brownian dynamics simulations of Hafezi et al..3 502 who have found that in binary mixed micelles, the inner micelle 503 cores are mainly occupied by the longer blocks; the shorter 504 core blocks are more concentrated in the outer parts of the 505 core. Finally, at smaller $\langle N_{\text{core}} \rangle$, the predicted R_c is noticeably 506 larger than that obtained from experiments for both sets of 507 calculations. Presumably, this is due to the fact that in this 508 regime, most of the core blocks are the shorter ones, which are, 509 therefore, still required to stretch to fill the entire space of the 510 core. Therefore, based on this analysis, we propose that in the 511 binary mixed spherical micelles, the composition of the two 512 diblocks controls the relative degree of deformation of the 513 shorter core block. In other words, the partial or complete 514 release of the shorter core block stretching due to the presence 515 of the longer ones leads to a larger aggregation number and, 516 thus, a larger micelle dimension in the binary mixed micelles, 517 which is significantly larger than the pure micelles at the same 518 $\langle N_{\rm core} \rangle$. In fact, self-consistent field theory also predicts less s19 stretched chain conformations for mixed long and short block 520 co-polymers in the melt. Additionally, it has been 521 reported in block co-polymer melts by both experiment and 522 theory that the domain spacing increases with increasing 523 polydispersity at a fixed average chain length. 69,70 This is 524 understood based on the idea that disperse co-polymers release 525 part of the stretching energy of the chains. All these results are 526 conceptually in line with the interpretation presented here.

One important assumption made in the calculations is that the two diblocks are fully mixed on the molecular level, i.e., there is a single population of mixed micelles with an identical average composition of the two diblocks. Several pieces of evidence support this assumption. First, we compared the SANS scattering traces of two micelle solutions formed with diblocks of (25–24) and (25–53) in partially deuterated [EMIM][TFSI] (Figure S9). The two samples have identical

content but were prepared in two different ways. One of them 535 was prepared following the same protocol as described above 536 (i.e., premixing), which yielded binary mixed micelles of (25-537 24) + (25-53); the other one was prepared by first forming 538 the individual micelle solutions of (25-24) and (25-53), 539 respectively, which were then mixed in a predetermined ratio 540 (i.e., postmixing). As shown in Figure S9, the scattering traces 541 of these two samples are very different especially in the middle 542 q range. Specifically, one sees a clear first q minimum in the 543 binary mixed micelles but not in the blend of single diblock 544 micelle solutions, which instead displays a broad bump. This 545 result strongly implies co-micellization of the two diblocks in 546 the premixing protocol.⁴⁷ It might be noted that the cosolvent 547 premixing protocol adopted here for micelle preparation could 548 facilitate the hybridization of the two diblocks during 549 micellization. As the evaporation of the co-solvent is relatively 550 fast, the two diblocks will assemble into micelles roughly at the 551 same time, leading to the formation of well-mixed micelles. 552 This is in contrast with the postmixing protocol and the 553 temperature jump/ramp from the unimer to micelle regime, 554 often adopted in the literature, which could form different 555 populations of micelles, depending on the molecular exchange 556 kinetics. Second, as mentioned earlier, there is only a single 557 narrow size peak observed from the DLS data for the mixed 558 micelles. In fact, the dispersity of the hydrodynamic radius μ_2 / 559 Γ^2 is always smaller than 0.1 (Figure S3, comparable to the 560 values of the pure micelle solutions), indicating that the 561 distribution of the mixed micelle size is relatively narrow. 562 Similar observations were made by Honda et al. 42 Third, as 563 shown in Figure 3, the coefficient of variation in R_c (σ_R/R_c) 564 from SAXS of the binary mixed micelles is comparable or even 565 smaller than that of the single diblock micelles (except when 566 the mole fraction of the longer diblock is smaller than 30%). 567 This suggests very similar core size distributions between the 568 binary mixed and pure micelles.

We have noted that the micelle core dimension is more 570 disperse at small mole fractions of the longer diblock (i.e., 571 <30%) and presents an apparent maximum at ~15 mol % 572 (Figure 3). If one looks closely at the scattering profiles 573 (Figures 1b,c, and S6) in this co-polymer composition regime, 574 the first q minimum is relatively shallow, i.e., a broader 575 distribution for the core radius. Several possible explanations 576 could be suggested. First, there is frustration of shorter and 577 longer core block packing within this composition window, 578 yielding two populations of micelles with slightly different 579 compositions of the two diblocks. 35,37,39 Apparently, even this 580 is true, the difference in the micelle dimensions between the 581 two populations is so small that it cannot be resolved in 582 experiments. 37,40 On the other hand, it is likely that there is 583 fluctuation in the composition of the two diblocks among 584 distinct mixed micelles;³⁸ this composition fluctuation brings 585 more variation in the core radius of smaller micelles, i.e., when 586 $\langle N_{\rm core} \rangle$ is smaller. To elaborate on this, the following 587 calculations were performed. We added different mole 588 fractions of longer diblocks to a certain number of 589 monodisperse pure smaller micelles. Similarly, different mole 590 fractions of the shorter diblocks were added to monodisperse 591 pure larger micelles. Assume that the number of longer or 592 shorter diblocks incorporated into distinct micelles follows 593 Gaussian statistics, the distribution of the micelle core size after 594 the incorporation of various numbers of the other diblocks can 595 be determined. Two sets of calculations were conducted: in 596 one, the CV in the number of the other diblocks assigned to 597

598 one micelle was fixed, whereas in the other, a constant standard 599 deviation was assumed. The results are summarized in Figure 600 S10. As shown there, in both cases, the CV of core radius in 601 the smaller micelles incorporating low fractions of longer 602 diblocks is significantly larger than that in the larger micelles 603 upon addition of the same fraction of shorter diblocks. This is 604 qualitatively consistent with the results in Figure 3. All these 605 factors need to be considered to understand the variation in 606 the R_c distribution of the binary mixed micelles with co-607 polymer composition. Nevertheless, it is reasonable to 608 conclude that the two diblocks co-micellize into binary 609 mixed micelles in a concerted fashion. The same conclusion 610 was drawn by Jain et al., who had used a similar premixing 611 protocol to prepare binary mixed diblock co-polymer micelles 612 and argued that the two BCPs are uniformly distributed across 613 all of the micelles.2

Another assumption embedded in the model is that the 615 binary mixed micelles adopt a spherical morphology, with a 616 uniform radius in all orientations. However, recent computer 617 simulation suggests that the mixed micelles could be 618 ellipsoidal, with the shorter chains straddling the core and 619 corona in the region of ellipsoidal interface that is closer to the 620 center of the micelle. Similar arguments were made by Liu et 621 al. to explain the thermodynamic stability of the Frank-Kasper 622 phases in bulk binary blends of diblock co-polymers.⁷¹ We 623 cannot rule this possibility out in the current system, but it 624 would be hard to discern experimentally. However, we believe 625 that the formation of ellipsoidal micelles (assume they do 626 exist) is another way to regulate the packing and the degree of 627 stretching of the two core blocks, which is conceptually in line 628 with the argument from our work. On the other hand, the 629 formation of ellipsoidal micelles requires the partial micro-630 phase separation of the two diblocks within the micelles, which 631 will decrease the mixing entropy of the system. Additionally, as 632 the difference between the two core blocks in our system is not 633 that large (the unperturbed radius of gyration differs by a 634 factor of ~ 1.5), the aspect ratio of the putative ellipsoidal 635 micelles should not be far from unity, i.e., still close to a 636 spherical shape. This is especially true for binary mixed 637 micelles with extreme proportions of the two diblocks. In fact, 638 Brownian dynamics simulations found that the relative shape 639 anisotropy is roughly the same between pure and mixed 640 micelles, especially for cases with long core blocks, 36,38 as studied here. Moreover, Yoo et al. performed TEM studies on 642 binary mixed micelles and showed that they adopt a nearly 643 spherical shape. 43 Note that in their system, the core block 644 length of the two diblocks differs by a factor of ~2.4, similar to 645 the case in our study $(N_{\text{core,L}}/N_{\text{core,S}} = 2.1-2.5)$.

Based on free-energy calculations, we have provided a quantitative explanation for the intriguing finding that mixed micelles have significantly larger dimensions than pure ones. It has been argued that in spherical micelles, the volume of the micelle core interior is rather small, so that only a few core blocks are necessarily deformed to fill the micelle core. From this perspective, these free-energy calculations might overestimate the core block stretching penalty. However, in the original derivation of the core block elastic energy in eqs 3 and for 6, the free ends of the core blocks are allowed to fluctuate within the entire space of the micelle core to provide a uniform for polymer density. Moreover, the assumption of uniform stretching for the core block indeed yields the correct scaling with the core block length (Figure S8). Therefore, these calculations should be appropriate. On the other hand, Zhulina

et al. have argued that the core elastic free energy is small 661 compared to the corona and interface terms even for crew-cut 662 micelles, and thus it does not strongly affect the micellar 663 structure. With the model parameters in Table S1, we 664 calculated the free energy per co-polymer chain in single 665 diblock micelles and found that, in the current system, the 666 core, corona, and interface contribute ~10, 30, and 60%, 667 respectively, to the total free energy. This result is qualitatively 668 consistent with that from Zhulina et al.; however, we have 669 found that even with this relatively small core elastic energy, 670 the micelle core dimension can still be significantly modified 671 (Figure 5). Specifically, Figure S11 shows that the micelle core 672 radius could differ by 20-30%, depending on the core block 673 length, if the core free energy is not taken into account in the 674 calculation. This further justifies the importance of core block 675 stretching in determining the structure of spherical micelles, 676 especially mixed ones, and these results provide new insight 677 into the co-micellization of binary diblock co-polymer mixtures 678 with distinct core block lengths.

One final aspect to be noted is the relative magnitude of 680 increase in $R_{\rm h}$ and $R_{\rm c}$ of the binary mixed micelles compared to 681 pure ones. Although both sizes are significantly larger for the 682 binary mixed micelles, the increase is more dramatic for $R_{\rm h}$ 683 than for R_c (Figure 2a,b). For instance, at $\langle N_{\rm core} \rangle \approx 370$, $\Delta R_{\rm b} = 684$ 5.5 nm is much larger than $\Delta R_{\rm c}$ = 3.3 nm, where $\Delta R_{\rm h}$ = $R_{\rm h,mixed}$ 685 $-R_{\rm h,pure}$, and $\Delta R_{\rm c}=R_{\rm c,mixed}-R_{\rm c,pure}$. Presumably, this is due to 686 the thicker corona for the binary mixed micelles. As shown in 687 Figure 4c, the aggregation number of the binary mixed micelles 688 is substantially larger than the pure ones at the same $\langle N_{\text{core}} \rangle$, 689 which even displays a maximum as a function of $\langle N_{\rm core} \rangle$. 690 Considering that the corona block length of the two diblocks is 691 the same, a larger aggregation number will impose higher steric 692 repulsion among the chains in the corona. As a result, the 693 corona chains could be more stretched, leading to a larger 694 corona thickness (Figure S12) and, therefore, a larger increase 695 in R_h than R_c .

SUMMARY 697

In this report, we have examined the structure of micelles 698 formed with binary diblock co-polymer mixtures with the same 699 $N_{
m corona}$ but different $N_{
m core}$. The micelles were prepared via a co- 700 solvent protocol. We have found that the two diblocks can co-701 micellize and form a single, relatively monodisperse population 702 of mixed micelles. DLS and SAXS measurements show that the 703 average dimensions (both $R_{\rm h}$ and $R_{\rm c}$) of the mixed micelles 704 monotonically increase with the fraction of the longer diblock 705 in the co-polymer mixture; however, R_c vs $\langle N_{core} \rangle$ for the 706 mixed micelles does not follow a simple power law as in the 707 case of single diblock micelles. Additionally, the aggregation 708 number extracted from the SANS data first increases and then 709 decreases with $\langle N_{\rm core} \rangle$, in contrast to the monotonic increase in 710 the case of single diblock micelles. Interestingly, the 711 dimensions and aggregation numbers of the binary mixed 712 micelles assume significantly larger values than that formed 713 with single diblocks at the same $\langle N_{\rm core} \rangle$. Free-energy analysis 714 was performed to predict the micelle core dimensions at 715 equilibrium. The calculation shows excellent agreement with 716 the experimentally measured values of R_c in single diblock 717 micelles. However, it significantly underestimates the core sizes 718 of the binary mixed micelles when both the shorter and longer 719 core blocks are uniformly stretched to fill the micelle core. 720 Importantly, if the elastic free energy of the shorter core blocks 721 is eliminated, the predicted values of R_c match well with 722

723 experiments. Combining experiments and calculations, we 724 propose that the shorter core blocks are, to some degree, 725 relaxed in the micelle core in the presence of the longer ones, 726 which will predominantly occupy the central space of the 727 micelle core. This partial or complete release of the shorter 728 core block stretching thermodynamically favors micelles with a 729 larger aggregation number and, thus, a larger micelle 730 dimension. These results underscore the fact that the 731 molecular packing of the two core blocks with distinct lengths 732 within a spherical micelle core is a critical factor dictating the 733 thermodynamic structure of the mixed micelles. Moreover, this 734 work demonstrates that the micellar structure (core radius, 735 aggregation number, corona thickness) can be facilely and 736 precisely tuned by blending various proportions of two diblock 737 co-polymers.

ASSOCIATED CONTENT

Supporting Information

740 The Supporting Information is available free of charge on the 741 ACS Publications website at DOI: 10.1021/acs.macro-742 mol.9b00613.

> SEC traces, additional DLS data, comparison of R_c from Pedersen model fits and the characteristic equation for the minima in q, additional SAXS profiles, estimation of the solvent volume fraction in the micelle core, calculation of free-energy model parameters, comparison of calculations and experiments for single diblock copolymer micelles, comparison of the SANS traces of two micelle solutions prepared by two different protocols, calculation of coefficient of variation in the micelle core radius upon incorporation of a second diblock (Figures S1-S12 and Table S1) (PDF)

AUTHOR INFORMATION

755 Corresponding Author

756 *E-mail: lodge@umn.edu.

757 **ORCID** ®

743

744

746

749

750

751

752

753

758 Dan Zhao: 0000-0001-8928-0691 759 En Wang: 0000-0002-3271-7562

760 Timothy P. Lodge: 0000-0001-5916-8834

762 The authors declare no competing financial interest.

ACKNOWLEDGMENTS

764 The authors acknowledge financial support from National 765 Science Foundation (DMR-1707578). Portions of this work 766 were performed at the DuPont-Northwestern-Dow Collabo-767 rative Access Team (DND-CAT) located at Sector 5 of the 768 Advanced Photon Source (APS). DND-CAT is supported by 769 Northwestern University, E.I. DuPont de Nemours and Co., 770 and The Dow Chemical Company. This research used 771 resources of the Advanced Photon Source, a U.S. Department 772 of Energy (DOE) Office of Science User Facility operated for 773 the DOE Office of Science by Argonne National Laboratory 774 under Contract No. DE-AC02-06CH11357. We acknowledge 775 the support of the National Institute of Standards and 776 Technology (NIST), U.S. Department of Commerce, in providing the neutron research facilities used in this work. 778 We would like to thank Dr Yimin Mao and Dr Paul Butler for 779 their assistance in SANS measurements. We thank Dr David 780 Morse and Dr Michael Rubinstein for helpful discussions.

REFERENCES

- (1) Bang, J.; Jain, S.; Li, Z.; Lodge, T. P.; Pedersen, J. S.; Kesselman, 782 E.; Talmon, Y. Sphere, cylinder, and vesicle nanoaggregates in 783 poly(styrene-b-isoprene) diblock copolymer solutions. Macromolecules 784 2006, 39, 1199-1208.
- (2) He, Y.; Li, Z.; Simone, P.; Lodge, T. P. Self-assembly of block 786 copolymer micelles in an ionic liquid. J. Am. Chem. Soc. 2006, 128, 787 2745-2750.
- (3) Zhulina, E. B.; Adam, M.; LaRue, I.; Sheiko, S. S.; Rubinstein, M. 789 Diblock copolymer micelles in a dilute solution. Macromolecules 2005, 790 38, 5330-5351.
- (4) Kataoka, K.; Harada, A.; Nagasaki, Y. Block copolymer micelles 792 for drug delivery: design, characterization and biological significance. 793 Adv. Drug Delivery Rev. 2001, 47, 113-131. 794
- (5) Tyrrell, Z. L.; Shen, Y.; Radosz, M. Fabrication of micellar 795 nanoparticles for drug delivery through the self-assembly of block 796 copolymers. Prog. Polym. Sci. 2010, 35, 1128-1143.
- (6) Park, T. G.; Jeong, J. H.; Kim, S. W. Current status of polymeric 798 gene delivery systems. Adv. Drug Delivery Rev. 2006, 58, 467-486.
- (7) Attia, A. B. E.; Ong, Z. Y.; Hedrick, J. L.; Lee, P. P.; Ee, P. L. R.; 800 Hammond, P. T.; Yang, Y.-Y. Mixed micelles self-assembled from 801 block copolymers for drug delivery. Curr. Opin. Colloid Interface Sci. 802 2011, 16, 182-194.
- (8) Li, Z.; Lenk, T. I.; Yao, L. J.; Bates, F. S.; Lodge, T. P. 804 Maintaining hydrophobic drug supersaturation in a micelle corona 805 reservoir. Macromolecules 2018, 51, 540-551.
- (9) Glass, R.; Möller, M.; Spatz, J. P. Block copolymer micelle 807 nanolithography. Nanotechnology 2003, 14, 1153-1160.
- (10) Vriezema, D. M.; Comellas Aragonès, M.; Elemans, J. A. A. W.; 809 Cornelissen, J. J. L. M.; Rowan, A. E.; Nolte, R. J. M. Self-assembled 810 nanoreactors. Chem. Rev. 2005, 105, 1445-1490.
- (11) Wright, D. B.; Patterson, J. P.; Pitto-Barry, A.; Lu, A.; Kirby, N.; 812 Gianneschi, N. C.; Chassenieux, C.; Colombani, O.; O'Reilly, R. K. 813 The copolymer blending method: a new approach for targeted 814 assembly of micellar nanoparticles. Macromolecules 2015, 48, 6516-815
- (12) Wever, D.; Picchioni, F.; Broekhuis, A. Polymers for enhanced 817 oil recovery: a paradigm for structure-property relationship in 818 aqueous solution. Prog. Polym. Sci. 2011, 36, 1558-1628.
- (13) Raffa, P.; Broekhuis, A. A.; Picchioni, F. Polymeric surfactants 820 for enhanced oil recovery: a review. J. Pet. Sci. Eng. 2016, 145, 723-821
- (14) Pavia-Sanders, A.; Zhang, S.; Flores, J. A.; Sanders, J. E.; 823 Raymond, J. E.; Wooley, K. L. Robust magnetic/polymer hybrid 824 nanoparticles designed for crude oil entrapment and recovery in 825 aqueous environments. ACS Nano 2013, 7, 7552-7561.
- (15) de AA Soler-Illia, G. J.; Crepaldi, E. L.; Grosso, D.; Sanchez, C. 827 Block copolymer-templated mesoporous oxides. Curr. Opin. Colloid 828 Interface Sci. 2003, 8, 109-126.
- (16) Lu, M.; Chen, F.; Cao, C.; Garvey, C. J.; Fletcher, N. L.; 830 Houston, Z. H.; Lu, H.; Lord, M. S.; Thurecht, K. J.; Stenzel, M. H. 831 Importance of polymer length in fructose-based polymeric micelles for 832 an enhanced biological activity. Macromolecules 2019, 52, 477-486. 833
- (17) Choi, S.-H.; Bates, F. S.; Lodge, T. P. Structure of poly 834 (styrene-b-ethylene-alt-propylene) diblock copolymer micelles in 835 squalane. J. Phys. Chem. B 2009, 113, 13840-13848.
- (18) LaRue, I.; Adam, M.; Zhulina, E. B.; Rubinstein, M.; Pitsikalis, 837 M.; Hadjichristidis, N.; Ivanov, D. A.; Gearba, R. I.; Anokhin, D. V.; 838 Sheiko, S. S. Effect of the soluble block size on spherical diblock 839 copolymer micelles. Macromolecules 2008, 41, 6555-6563.
- (19) Wang, E.; Lu, J.; Bates, F. S.; Lodge, T. P. Effect of corona 841 block length on the structure and chain exchange kinetics of block 842 copolymer micelles. Macromolecules 2018, 51, 3563-3571.
- (20) Zhang, L.; Eisenberg, A. Multiple morphologies of "crew-cut" 844 aggregates of polystyrene-b-poly (acrylic acid) block copolymers. 845 Science 1995, 268, 1728-1731.
- (21) Chaibundit, C.; Ricardo, N. M.; Costa, F. dM.; Yeates, S. G.; 847 Booth, C. Micellization and gelation of mixed copolymers P123 and 848 F127 in aqueous solution. Langmuir 2007, 23, 9229-9236.

I

- 850 (22) Zhang, M.; Djabourov, M.; Bourgaux, C.; Bouchemal, K. 851 Nanostructured fluids from pluronic mixtures. *Int. J. Pharm.* **2013**, 852 454, 599–610.
- 853 (23) Liu, T.; Nace, V. M.; Chu, B. Self-assembly of mixed 854 amphiphilic triblock copolymers in aqueous solution. *Langmuir* 855 **1999**, *15*, 3109–3117.
- 856 (24) El Asmar, A.; Gimello, O.; Morandi, Gl.; Le Cerf, D.; Lapinte, 857 V.; Burel, F. Tuning the thermo-sensitivity of micellar systems
- 858 through a blending approach. Macromolecules 2016, 49, 4307-4315.
- 859 (25) Renou, F.; Nicolai, T.; Nicol, E.; Benyahia, L. Structure and 860 viscoelasticity of mixed micelles formed by poly(ethylene oxide) end 861 capped with alkyl groups of different length. *Langmuir* **2009**, 25, 515—862 521.
- 863 (26) Jain, S.; Bates, F. S. Consequences of nonergodicity in aqueous 864 binary PEO-PB micellar dispersions. *Macromolecules* **2004**, *37*, 865 1511–1523.
- 866 (27) Zhu, J.; Zhang, S.; Zhang, K.; Wang, X.; Mays, J. W.; Wooley, 867 K. L.; Pochan, D. J. Disk-cylinder and disk-sphere nanoparticles via a 868 block copolymer blend solution construction. *Nat. Commun.* **2013**, *4*, 869 No. 2297.
- 870 (28) Cho, A.; La, Y.; Jeoung, S.; Moon, H. R.; Ryu, J.-H.; Shin, T. J.; 871 Kim, K. T. Mix-and-match assembly of block copolymer blends in 872 solution. *Macromolecules* **2017**, *50*, 3234–3243.
- 873 (29) Procházka, K.; Martin, T. J.; Webber, S. E.; Munk, P. Onion-874 type micelles in aqueous media. *Macromolecules* **1996**, 29, 6526—875 6530.
- 876 (30) Zhang, W.; Shi, L.; Gao, L.; An, Y.; Wu, K. Formation of core-877 shell-corona micellar complexes through adsorption of double 878 hydrophilic diblock copolymers into core-shell micelles. *Macromol.* 879 *Ravid Commun.* **2005**, 26, 1341–1345.
- 880 (31) Srinivas, G.; Pitera, J. W. Soft patchy nanoparticles from 881 solution-phase self-assembly of binary diblock copolymers. *Nano Lett.* 882 **2008**, *8*, 611–618.
- 883 (32) Kang, N.; Perron, M.-È.; Prud'Homme, R. E.; Zhang, Y.; 884 Gaucher, G.; Leroux, J.-C. Stereocomplex block copolymer micelles: 885 core-shell nanostructures with enhanced stability. *Nano Lett.* **2005**, *5*, 886 315–319.
- 887 (33) Sens, P.; Marques, C.; Joanny, J.-F. Mixed micelles in a 888 bidisperse solution of diblock copolymers. *Macromolecules* **1996**, 29, 889 4880–4890.
- 890 (34) Shim, D.; Marques, C.; Cates, M. Diblock copolymers: 891 comicellization and coadsorption. *Macromolecules* **1991**, 24, 5309—892 5314.
- 893 (35) Borovinskii, A. L.; Khokhlov, A. R. Micelle formation in the 894 dilute solution mixtures of block-copolymers. *Macromolecules* **1998**, 895 *31*, 7636–7640.
- 896 (36) Hafezi, M.-J.; Sharif, F. Brownian dynamics simulation of 897 amphiphilic block copolymers with different tail lengths, comparison 898 with theory and comicelles. *J. Mol. Graphics Modell.* **2015**, *62*, 165–899 173.
- 900 (37) Prhashanna, A.; Khan, S. A.; Chen, S. B. Co-micellization 901 behavior in poloxamers: dissipative particle dynamics study. *J. Phys.* 902 *Chem. B* **2015**, *119*, 572–582.
- 903 (38) Hafezi, M.-J.; Sharif, F. Brownian dynamics simulation of 904 comicellization of amphiphilic block copolymers with different tail 905 lengths. *Langmuir* **2012**, *28*, 16243–16253.
- 906 (39) Gaisford, S.; Beezer, A. E.; Mitchell, J. C. Diode-array UV 907 spectrometric evidence for cooperative interactions in binary mixtures 908 of pluronics F77, F87, and F127. *Langmuir* 1997, 13, 2606–2607.
- 909 (40) Pragatheeswaran, A. M.; Chen, S. B.; Chen, C.-F.; Chen, B.-H. 910 Micellization and gelation of PEO-PPO-PEO binary mixture with 911 non-identical PPO block lengths in aqueous solution. *Polymer* **2014**, 912 *55*, 5284–5291.
- 913 (41) Mingvanish, W.; Chaibundit, C.; Booth, C. Mixed micellisation 914 of oxyethylene-oxybutylene diblock and triblock copolymers in water 915 studied by light scattering. *Phys. Chem. Chem. Phys.* **2002**, *4*, 778–784. 916 (42) Honda, C.; Yamamoto, K.; Nose, T. Comicellization of binary 917 mixtures of block copolymers with different block lengths in a 918 selective solvent. *Polymer* **1996**, *37*, 1975–1984.

- (43) Yoo, S. I.; Sohn, B.-H.; Zin, W.-C.; Jung, J. C.; Park, C. 919 Mixtures of diblock copolymer micelles by different mixing protocols. 920 *Macromolecules* **2007**, *40*, 8323–8328.
- (44) Koňák, Č.; Helmstedt, M. Comicellization of diblock and 922 triblock copolymers in selective solvents. *Macromolecules* **2003**, *36*, 923 4603–4608.
- (45) Pacovská, M.; Prochazka, K.; Tuzar, Z.; Munk, P. Formation of 925 block copolymer micelles: a sedimentation study. *Polymer* **1993**, 34, 926 4585–4588.
- (46) Esselink, F.; Dormidontova, E.; Hadziioannou, G. Redistrib- 928 ution of block copolymer chains between mixed micelles in solution. 929 *Macromolecules* **1998**, *31*, 4873–4878. 930
- (47) Xie, R.; López-Barrón, C. R.; Greene, D. G.; Wagner, N. J. 931 Comicellization of binary PEO-PPO-PEO triblock copolymer 932 mixtures in ethylammonium nitrate. *Macromolecules* **2018**, *51*, 933 1453–1461.
- (48) Koňák, Č.; Helmstedt, M. Comicellization of chemically 935 identical diblock copolymers with different molecular parameters of 936 the constituent blocks in a selective solvent. *Macromolecules* **2001**, 34, 937 6131–6133.
- (49) König, N.; Willner, L.; Pipich, V.; Zinn, T.; Lund, R. 939 Cooperativity during melting and molecular exchange in micelles 940 with crystalline cores. *Phys. Rev. Lett.* **2019**, *122*, No. 078001.
- (50) Newby, G. E.; Hamley, I. W.; King, S. M.; Martin, C. M.; 942 Terrill, N. J. Structure, rheology and shear alignment of Pluronic 943 block copolymer mixtures. *J. Colloid Interface Sci.* **2009**, 329, 54–61. 944
- (51) Hoarfrost, M. L.; He, Y.; Lodge, T. P. Lower critical solution 945 temperature phase behavior of poly(*n*-butyl methacrylate) in ionic 946 liquid mixtures. *Macromolecules* **2013**, *46*, 9464–9472.
- (52) Ma, Y.; Lodge, T. P. Poly(methyl methacrylate)-block-poly(n-948 butyl methacrylate) diblock copolymer micelles in an ionic liquid: 949 Scaling of core and corona size with core block length. *Macromolecules* 950 **2016**, 49, 3639–3646.
- (53) Ma, Y. Structure and Chain Exchange Kinetics of Block 952 Copolymer Micelles in Selective Solvents. Doctoral Thesis, University 953 of Minnesota, 2017. 954
- (54) Wiley, R. H.; Brauer, G. Refractometric determination of 955 second-order transition temperatures in polymers. II. Some acrylic, 956 vinyl halide, and styrene polymers. *J. Polym. Sci., Part A: Polym. Chem.* 957 **1948**, 3, 455–461.
- (55) Wright, D. B.; Patterson, J. P.; Gianneschi, N. C.; Chassenieux, 959 C.; Colombani, O.; O'Reilly, R. K. Blending block copolymer micelles 960 in solution; obstacles of blending. *Polym. Chem.* **2016**, *7*, 1577–1583. 961
- (56) Halperin, A.; Tirrell, M.; Lodge, T. P. Tethered chains in 962 polymer microstructures. *Adv. Polym. Sci.* **1992**, *100*, 31–71.
- (57) Birshtein, T.; Zhulina, E. Scaling theory of supermolecular 964 structures in block copolymer-solvent systems: 1. Model of micellar 965 structures. *Polymer* **1989**, *30*, 170–177.
- (58) Jakeš, J. Regularized positive exponential sum (REPES) 967 program A way of inverting Laplace transform data obtained by 968 dynamic light scattering. *Collect. Czech. Chem. Commun.* **1995**, *60*, 969 1781–1797.
- (59) Pedersen, J. S. Determination of size distribution from small- 971 angle scattering data for systems with effective hard-sphere 972 interactions. *J. Appl. Crystallogr.* **1994**, 27, 595–608.
- (60) Pedersen, J. S.; Gerstenberg, M. C. The structure of P85 974 Pluronic block copolymer micelles determined by small-angle neutron 975 scattering. *Colloids Surf., A* **2003**, 213, 175–187.
- (61) Pedersen, J. S.; Svaneborg, C.; Almdal, K.; Hamley, I. W.; 977 Young, R. N. A small-angle neutron and X-ray contrast variation 978 scattering study of the structure of block copolymer micelles: Corona 979 shape and excluded volume interactions. *Macromolecules* 2003, 36, 980 416–433.
- (62) Kline, S. R. Reduction and analysis of SANS and USANS data 982 using IGOR Pro. J. Appl. Crystallogr. 2006, 39, 895–900. 983
- (63) Zhao, D.; Ma, Y.; Lodge, T. P. Exchange kinetics for a single 984 block copolymer in micelles of two different sizes. *Macromolecules* 985 **2018**, *51*, 2312–2320.

987 (64) Semenov, A. N. Contribution to the theory of microphase 988 layering in block-copolymer melts. *Sov. Phys. JETP* **1985**, *61*, 733–989 742.

- 990 (65) Helfand, E.; Sapse, A. M. Theory of unsymmetric polymer– 991 polymer interfaces. *J. Chem. Phys.* **1975**, *62*, 1327–1331.
- 992 (66) Zhulina, E. B.; Birshtein, T. M. Theory of supermolecular
- 993 structures in polydisperse block copolymers: 2. Lamellar super-994 structure consisting of two-block copolymers. *Polymer* **1991**, 32, 995 1299–1308.
- 996 (67) Zhulina, E. B.; Lyatskaya, Y. V.; Birshtein, T. M. Theory of 997 supermolecular structures in polydisperse block copolymers: 3.
- 998 Cylindrical layers of bidisperse chains. *Polymer* **1992**, 33, 332–342. 999 (68) Lyatskaya, J. V.; Zhulina, E. B.; Birshtein, T. M. Theory of
- 1000 supermolecular structures in polydisperse block copolymers: 4.
- 1001 Cylindrical domains in binary mixtures of diblock copolymers and 1002 cylinder-lamellae transition. *Polymer* **1992**, *33*, 343–351.
- 1003 (69) Lynd, N. A.; Hillmyer, M. A. Influence of polydispersity on the 1004 self-assembly of diblock copolymers. *Macromolecules* **2005**, *38*, 8803–1005 8810.
- 1006 (70) Cooke, D. M.; Shi, A. C. Effects of polydispersity on phase 1007 behavior of diblock copolymers. *Macromolecules* **2006**, *39*, 6661–1008 6671.
- 1009 (71) Liu, M.; Qiang, Y.; Li, W.; Qiu, F.; Shi, A.-C. Stabilizing the 1010 Frank-Kasper phases via binary blends of AB diblock copolymers. 1011 ACS Macro Lett. **2016**, *5*, 1167–1171.